J|A|C|S
ARTICLES
Published on Web 03/15/2005

Effect of $SOCl_2$ Treatment on Electrical and Mechanical Properties of Single-Wall Carbon Nanotube Networks

Urszula Dettlaff-Weglikowska,*,† Viera Skákalová,† Ralf Graupner,‡ Sung Ho Jhang,§ Byung Hoon Kim,§ Hyun Jung Lee,§ Lothar Ley,‡ Yung Woo Park,§ Savas Berber,||,# David Tománek,|| and Siegmar Roth†

Contribution from the Max-Planck-Institute for Solid State Research, Heisenbergstr.1, D-70569 Stuttgart, Germany, Institute of Technical Physics, University of Erlangen, Erwin-Rommel Strasse 1, D-91058 Erlangen, Germany, School of Physics and Condensed Matter Research Institute, Seoul National University, Seoul, 151-747, Korea, and Physics and Astronomy Department, Michigan State University, East Lansing, Michigan 48824-2320

Received June 5, 2004; E-mail: u.dettlaff@fkf.mpg.de

Abstract: Chemical modification by $SOCl_2$ of an entangled network of purified single-wall carbon nanotubes, also known as 'bucky paper', is reported to profoundly change the electrical and mechanical properties of this system. Four-probe measurements indicate a conductivity increase by up to a factor of 5 at room temperature and an even more pronounced increase at lower temperatures. This chemical modification also improves the mechanical properties of SWNT networks. Whereas the pristine sample shows an overall semiconducting character, the modified material behaves as a metal. The effect of $SOCl_2$ is studied in terms of chemical doping of the nanotube network. We identified the microscopic origin of these changes using SEM, XPS, NEXAFS, EDX, and Raman spectroscopy measurements and ab initio calculations. We interpret the $SOCl_2$-induced conductivity increase by *p*-type doping of the pristine material. This conclusion is reached by electronic structure calculations, which indicate a Fermi level shift into the valence band, and is consistent with the temperature dependence of the thermopower.

1. Introduction

Electrical and mechanical properties of carbon nanotubes are of high interest for a variety of applications, ranging from nanoelectronics and nanoelectromechanical systems (NEMS) to nanocomposites.[1] A vast number of chemical treatments has been applied successfully to solve,[2] disperse,[3−6] functionalize,[7−16] or chemically dope carbon nanotubes.[17−29] The objective of these treatments was to enhance the conductivity of intrinsically

* To whom correspondence should be addressed.
† Max-Planck-Institute for Solid State Research.
‡ University of Erlangen.
§ Seoul National University.
|| Michigan State University.
Present address: Institute of Physics, University of Tsukuba, 1-1-1 Tennodai, Tsukuba, Ibaraki 305-8571, Japan.

(1) In *Carbon Nanotubes: Synthesis, Structure, Properties and Applications;* Dresselhaus, M. S., Dresselhaus, G., Avouris, P., Eds.; Topics in Applied Physics 80; Springer: New York, 2001.
(2) Hamon, M. A.; Chen, J.; Hu, H.; Chen, Y.; Itkis, M. E.; Rao, A. M.; Ecklund, P. C.; Haddon, R. C. *Adv. Mater.* **1999**, *11*, 834−839.
(3) O'Connell, M. J.; Bachilo, S. M.; Huffman, C. B.; Moore, V. C.; Strano, M. S.; Haroz, E. H.; Rialon, K. L.; Boul, P. J.; Noon, W. H.; Kittrell, C.; Ma, J. P.; Hauge, R. H.; Weisman, R. B.; Smalley, R. E. *Science* **2002**, *297*, 593−596.
(4) Bachilo, S. M.; Strano, M. S.; Kittrell, C.; Hauge, R. H.; Smalley, R. E.; Weisman, R. B. *Science* **2002**, *298*, 2361−2366.
(5) Davis, V. A.; Ericson, L. M.; Parra-Vasques, A. N. G.; Fan, H.; Wang, Y.; Prieto, V.; Longoria, J. A.; Ramesh, S.; Saini, R. K.; Kittrell, C.; Billups, W. E.; Adams, W. W.; Hauge, R. H.; Smalley, R. E.; Pasqualli, M. *Macromolecules* **2004**, *37*, 154−160.
(6) Ramesh, S.; Ericson, L. M.; Davis, V. A.; Saini, R. K.; Kittrell, C.; Pasqualli, M.; Billups, W. E.; Adams, W. W.; Hauge, R. H.; Smalley, R. E. *J. Phys. Chem. B* **2004**, *108*, 8794−8798.
(7) Bahr, J. L.; Tour, J. M. *Chem. Mater.* **2001**, *13*, 3823−3824.
(8) Dyke, C. A.; Tour, J. M. *Nano Lett.* **2003**, *3*, 1215−1518.
(9) Strano, M. S.; Dyke, C. A.; Usrey, M. L.; Barone, P. W.; Allen, M. J.; Shan, H. W.; Kittrell, C.; Hauge, R. H.; Tour, J. M.; Smalley, R. E. *Science* **2003**, *301*, 1519−1522.
(10) Strano, M. S.; Huffman, C. B.; Moore, V. C.; O'Connell, M. J.; Haroz, E. H.; Hubbard, J.; Miller, M.; Rialon, K.; Kittrell, C.; Ramesh, S.; Hauge, R. H.; Smalley, R. E. *J. Phys. Chem. B* **2003**, *107*, 6979−6985.
(11) Hu, H.; Zhao, B.; Hamon, M. A.; Kamaras, K.; Itkis, M. E.; Haddon, R. C. *J. Am. Chem. Soc.* **2003**, *125*, 14893−14900.
(12) Holzinger, M.; Abraham, J.; Whelan, P.; Graupner, R.; Ley, L.; Hennrich, F.; Kappes, M.; Hirsch, A. *J. Am. Chem. Soc.* **2003**, *125*, 8566−8580.
(13) Liang, F.; Sadana, A. K.; Peera, A.; Chattopadhyay, J.; Gu, Z.; Hauge, R. H.; Billups, W. E. *Nano Lett.* **2004**, *4*, 1257−1260.
(14) Chen, J.; Rao, A. M.; Lyuksyutov, S.; Itkis, M. E.; Hamon, M. A.; Hu, H.; Cohn, R. W.; Eklund, P. C.; Colbert, D. T.; Smalley, R. E.; Haddon, R. C. *J. Phys. Chem. B* **2001**, *105*, 2525−2528.
(15) Chen, J.; Hamon, M. A.; Hu, H.; Chen, Y.; Rao, A. M.; Eklund, P. C.; Haddon, R. C. *Science* **1998**, *282*, 95−98.
(16) Mickelson, E. T.; Huffman, C. B.; Rinzler, A. G.; Smalley, R. E.; Hauge, R. H.; Margrave, J. L. *Chem. Phys. Lett.* **1998**, *296*, 188−194.
(17) Lee, R. S.; Kim, H. J.; Fischer, J. E.; Thess, A.; Smalley, R. E. *Nature* **1997**, *388*, 255−257.
(18) Lee, R. S.; Kim, H. J.; Fischer, J. E.; Lefebvre, J.; Radosavljevic, M.; Hone, J.; Johnson, A. T. *Phys. Rev. B* **2000**, *61*, 4526−4529.
(19) Claye, A. S.; Fischer, J. E.; Huffman, C. B.; Rinzler, A. G.; Smalley, R. E. *J. Electrochem. Soc.* **2000**, *147*, 2845−2852.
(20) Rao, A. M.; Eklund, P. C.; Bandow, S.; Thess, A.; Smalley, R. E. *Nature* **1997**, *388*, 257−259.
(21) Rao, A. M.; Bandow, S.; Richter, E.; Eklund, P. C. *Thin Solid Films* **1998**, *331*, 141−147.
(22) Kong, J.; Franklin, N. R.; Zhou, C.; Chapline, M. G.; Peng, S.; Cho, K.; Dai, H. *Science* **2000**, *287*, 622−625.
(23) Collins, P. G.; Bradley, K.; Ishigami, M.; Zettl, A. *Science* **2000**, *287*, 1801−1804.
(24) Chen, R. J.; Franklin, N. R.; Kong, J.; Cao, J.; Tombler, T. W.; Zhang, Y.; Dai, H. *Appl. Phys. Lett.* **2001**, *79*, 2258−2260.
(25) Kong, J.; Dai, H. *J. Phys. Chem B* **2001**, *105*, 2890−2893.
(26) Shim, M.; Javey, A.; Kam, N. W. S.; Dai, H. *J. Am. Chem. Soc.* **2001**, *123*, 11512−11513.
(27) Graupner, R.; Abraham, J.; Vencelova, A.; Seyller, T.; Hennrich, F.; Kappes, M. M.; Hirsch, A.; Ley, L. *Phys. Chem. Chem. Phys.* **2003**, *5*, 5472−5476.

semiconducting nanotubes,[17−26] modify their band gap,[9,10,22−26] or separate semiconducting from metallic nanotubes.[9,30−32]

Chemical doping of single-wall carbon nanotubes (SWNTs) with electron donors or acceptors has been used to enhance their electrical conductivity in analogy to the well-known graphite intercalation compounds. Intercalation of K and Rb in bundled SWNTs[17−19] has been shown to soften the Raman-active high-frequency tangential vibration modes, providing evidence for *n*-doping of the nanotubes.[20,21] A similar charge transfer, resulting in *n*-doping of nanotubes, has been observed upon adsorption of amine molecules.[25,26] *p*-Type doping associated with I_2 and Br_2 intercalation of SWNT bundles has been observed to increase the conductivity significantly, accompanied by a change to a metallic temperature dependence of their conductance.[21] On the basis of C 1s core level shifts, a similar electron transfer, resulting in *p*-doping of nanotubes, occurs in nanotubes exposed to strong inorganic acids,[27] such as nitric and sulfuric acid, and SO_2 molecules.[28] Encapsulation of various organic molecules has been reported to cause either *n*-type or *p*-type doping of nanotubes.[29]

Thionyl chloride, $SOCl_2$, is a liquid organic solvent which has been commonly used in the end-group derivatization of SWNTs to connect open nanotube ends to long-chain amines[2,33,34] or biomolecules.[35] These studies paid very little attention to the effect of $SOCl_2$ on the physical properties of the nanotube system. Here, we investigate the effect of $SOCl_2$ exposure on the electrical and mechanical properties of entangled networks of SWNTs, which are often called 'bucky paper'. We observed a remarkable improvement of the electrical conductivity and mechanical properties due to chemical modification of SWNTs by $SOCl_2$. The microscopic effect of the chemical modification of nanotube networks has been characterized by SEM, XPS, NEXAFS, EDX, and Raman spectroscopy experiments and its origin elucidated by ab initio calculations.

2. Experimental Section

Purified SWNTs, produced by catalytic conversion of high-pressure CO over Fe particles (HiPco) at CNI, Houston, TX, have been used as delivered. For chemical modification we also used SWNTs from CNI, formed by laser ablation (LA), and nanotubes formed by arc discharge in our lab, which were purified by controlled thermal oxidation in air followed by washing in HCl. Our reference sample of bucky paper contains pristine SWNTs and was prepared by filtration of the nanotube suspension in sodium dodecyl sulfate (SDS). In our study we compare this reference sample to $SOCl_2$-modified bucky paper, which was prepared in two different ways. One treatment involved immersing the reference system in liquid $SOCl_2$ (Fluka) followed by drying in air. The alternate preparation method started with a suspension of SWNTs in $SOCl_2$, which was stirred at 45 °C for 24 h, filtered, and subsequently dried in air. $SOCl_2$ is a very corrosive agent that reacts vigorously with water and moisture, forming HCl and SO_2. It has to be handled carefully under a fume hood, similar to strong inorganic acids. We observed a remarkable reactivity of the nanotube material toward $SOCl_2$ and a weight uptake of up to 30% following $SOCl_2$ treatment. In the following discussion we will refer to either the pristine bucky paper reference sample or $SOCl_2$–modified bucky paper, produced in one of the two ways mentioned above.

X-ray photoelectron spectra (XPS) of the reference and modified samples were recorded using a spectrometer equipped with a monochromatized Al Kα X-ray source (1486.6 eV). The binding energy was measured with respect to the Fermi level, which was regularly calibrated by measuring the Au 4f core level binding energy and adjusting its $4f^{7/2}$ component to a binding energy of 84.00 eV. In a near-edge X-ray absorption fine structure (NEXAFS) experiment a tunable monochromatized synchrotron light source was used to excite electrons from atomic core levels to unoccupied or partially occupied valence electron states. Energy-dispersive X-ray analysis (EDX) was carried out using the Taunusstein-Neuhof EDX system, equipped with a S-UTW-Si (Li) detector. Raman spectra were registered using the red laser line at $\lambda = 632$ nm. The temperature dependence of the resistivity has been determined in the Janis variable-temperature cryogenic system in the temperature range from room temperature to $T = 1.4$ K. The resistance was measured by a standard DC method in a four-probe configuration using the Keithley 220 current source and sensitive Keithley 182 digital nanovoltmeters for voltage reading. The thermoelectric power of the samples was measured by an ac steady-state method with low frequency (~33 mHz). The observed temperature gradient across the sample was typically 1−2 K and monitored by the Chromel−Constantan thermocouple. The contribution of the Au or Pt wire to the voltage drop measurement was carefully calibrated using pure Pb (99.999%) in the temperature range from 10 to 300 K. By measuring ΔV and ΔT simultaneously using the digital voltmeters, the thermopower S was determined by $S_{\text{measured}} = \Delta V/\Delta T = S_{\text{sample}} - S_{\text{Au or Pt}}$. The Young's modulus was determined from the elastic part of the stress vs strain curve, measured by a force transducer up to 20 N (Hottinger Baldwin Messtechnik, type 52).

3. Theoretical Section

We performed ab initio density functional theory (DFT) calculations within the local density approximation (LDA) of $SOCl_2$ and SO molecules interacting with naphthalene and pyrene representing a carbon nanotube fragment. We used Troullier−Martins ab initio pseudopotentials to describe the interaction of valence electrons with atomic nuclei and core electrons and the Perdew−Zunger form of the exchange-correlation potential as implemented in the SIESTA code.[36,37] We used a double-ζ basis[38] and a 50 Ry energy cutoff in the plane-wave expansions of the electron density and potential, which is sufficient to achieve a total energy convergence of ≤1 meV/atom during the self-consistency iterations. We performed a full optimization of the systems modeling the chemically modified nanotube to determine the optimum adsorption geometry, the adsorption energy, and the charge redistribution following the chemical modification.

4. Results and Discussion

SEM images of the pristine reference bucky paper and the $SOCl_2$-modified bucky paper are presented in Figure 1. The $SOCl_2$-modified bucky paper samples generally showed the same physical properties, independent of the precise way in which they were prepared.

(28) Goldoni, A.; Larciprete, R.; Petaccia, L.; Lizzit, S. *J. Am. Chem. Soc.* **2003**, *125*, 11329−11333.
(29) Takenobu, T.; Takano, T.; Shiraishi, M.; Murakami, Y.; Ata, M.; Kataura, H.; Achiba, Y.; Iwasa, Y. *Nat. Mater.* **2003**, *2*, 683−688.
(30) Chen, Z.; Du, X.; Du, M.-H.; Rancken, C. D.; Cheng, H.-P.; Rinzler, A. G. *Nano Lett.* **2003**, *3*, 1245−1249.
(31) Chattopadhyay, D.; Galeska, L.; Papadimitrakopoulos, F. *J. Am. Chem. Soc.* **2003**, *125*, 3370−3375.
(32) Zheng, M.; Jagota, A.; Semke, E. D.; Diner, B. A.; McLean, R. S.; Lustig, S. R.; Richardson, R. E.; Tassi, N. G. *Nat. Mater.* **2003**, *2*, 338−342.
(33) Chiu, P. W.; Duesberg, G. S.; Dettlaff-Weglikowska, U.; Roth, S. *Appl. Phys. Lett.* **2002**, *80*, 3811−3813.
(34) Chiu, P. W.; Kaempgen, M.; Roth, S. *Phys. Rev. Lett.* **2004**, *92*, 246802−1−246802−2.
(35) Baker, S. E.; Lasseter, T. L.; Smith, L. M.; Hamers, R. J. *Mater. Res. Soc. Symp. Proc.* **2003**, *737*, *F4.6.1-F4.6.7*.
(36) Ordejón, P.; Artacho, E.; Soler, J. M. *Phys. Rev. B* **1996**, *53*, R10441−R10444.
(37) Sánchez-Portal, D.; Ordejón, P.; Artacho, E.; Soler, J. M. *Int. J. Quantum Chem.* **1997**, *65*, 453−461.
(38) We found our calculations converged within the double-ζ basis, which is the standard basis set within SIESTA.

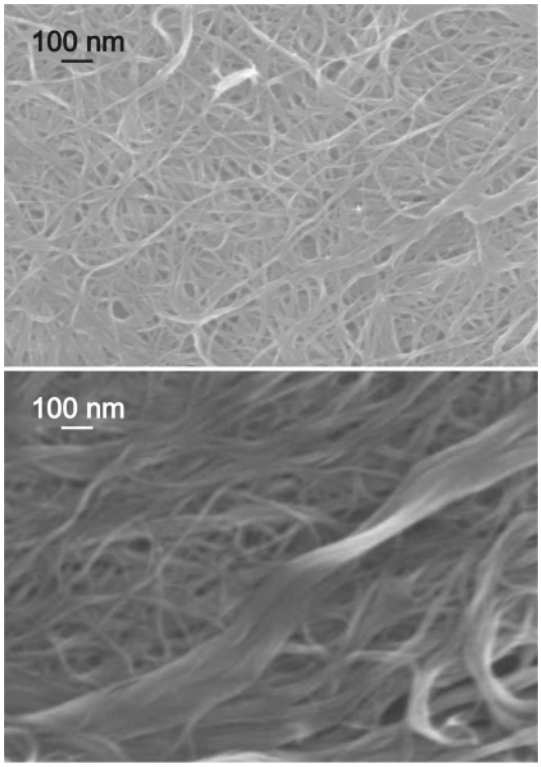

Figure 1. Scanning electron microscopy images of the pristine 'bucky paper' probe (top) and the modified probe, prepared from a suspension of nanotubes in $SOCl_2$ (bottom). The chemical treatment promotes aggregation to thicker nanotube bundles, thus enhancing the mechanical properties of the system.

Table 1. Observed Electrical Conductivity (S/cm) of Graphite (pellet) and SWNT Samples (bucky paper) at Room Temperature

sample	HiPco	LA	arc discharge	graphite
pristine	700	370	240	100
modified	3500	1200	960	120

Electrical Properties. The electrical conductivity of SWNTs increases with reaction time and saturates after about 24 h. In Table 1 we compare room-temperature four-probe electrical conductivity measurements for pristine and modified SWNT samples with those of graphite. Depending on the type of the sample, the room-temperature conductivity increases up to factor of 5 upon $SOCl_2$ exposure. The highest conductivity value, 3500 S/cm, was observed in modified HiPco SWNTs. This value is comparable to that of a single crystalline rope[39] and significantly higher than the previously reported conductivity of 0.78 S/cm in metal-enriched mats,[31] 160 S/cm in randomly oriented mats,[39] and 1100 S/cm in mats of magnetically aligned SWNTs.[40] The conductivity enhancement due to $SOCl_2$ was found to be less pronounced in the graphite sample (powder pressed into a pellet). The effect of $SOCl_2$ on the conductivity of nanotube networks also depends on the concentration of defects in the nanotube material. We observed an increase in the defect density upon γ-irradiation, which was accompanied by an enhanced electrical conductivity after $SOCl_2$ treatment.[41] We interpret the

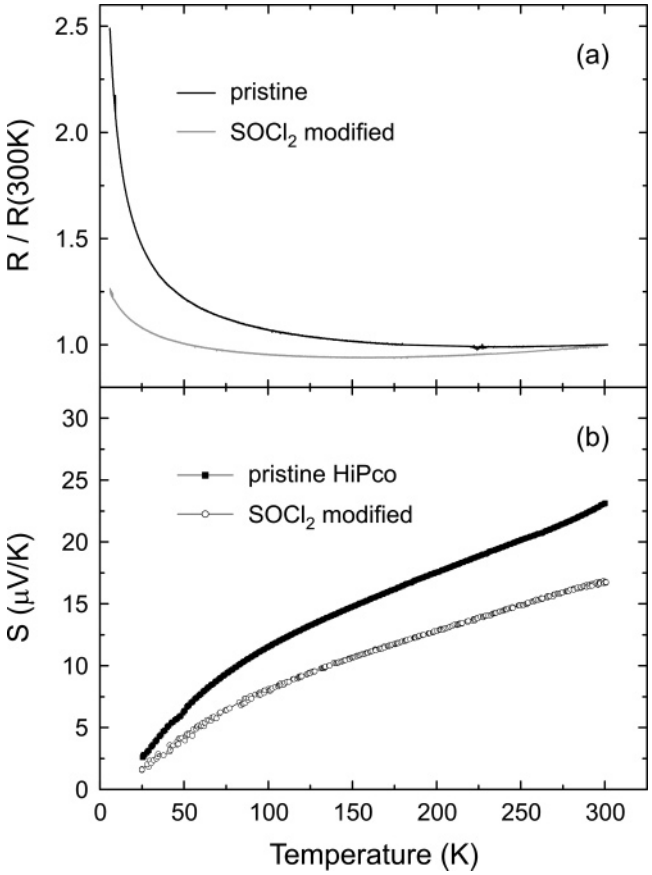

Figure 2. Temperature dependence of (a) resistance and (b) the thermoelectric power measured in SWNT networks. Results for the pristine material are shown in black; those for $SOCl_2$-modified HiPco material are shown in gray.

$SOCl_2$-induced conductivity enhancement by formation of SWNT/$SOCl_2$ charge-transfer complexes within the intercalated ropes, which improve the alignment of nanotube ropes in mats, as confirmed by the morphology changes in Figure 1.

The difference in the conductivity between pristine and functionalized samples becomes even more pronounced at low temperatures. The temperature dependence of the SWNT resistance is shown in Figure 2a. We plot R/R(300 K) to emphasize the difference in the behavior of the two systems at lower temperatures. These results show that the resistance of the pristine sample decreases continuously with increasing temperature, reflecting a semiconducting character of the sample. In the $SOCl_2$-treated sample, on the other hand, we observe a nonmetallic behavior only below 150 K. At higher temperatures we observe resistance increasing with increasing temperature, indicating a crossover to metallic behavior.

A similar temperature dependence has been described by a heterogeneous model proposed by Kaiser[42] involving regions of highly metallic conduction separated by barrier regions. The general characteristic of this conduction model, which has been developed for conducting polymers, is a change from a metallic to a nonmetallic behavior in the temperature dependence of the resistivity. Resistance of a metallic system increases with temperature, whereas the resistance of a nonconducting barrier decreases with increasing temperature and thermal energy. This leads to a crossover at a particular temperature, which depends

(39) Fisher, J. E.; Dai, H.; Thess, A.; Lee, R.; Hanjani, N. M.; Dehaas, D. L.; Smalley, R. E. *Phys. Rev. B* **1997**, *55*, R4921−R4924.
(40) Fisher, J. E.; Zhou, W.; Vavro, J.; Llaguno, M. C.; Guthy, C.; Haggenmueller, R.; Casavant, M. J.; Walters, D. E.; Smalley, R. E. *J. Appl. Phys.* **2003**, *93*, 2157−2163.
(41) Skakalova, V.; Dettlaff-Weglikowska, U.; Roth, S. *Diamond Relat. Mater.* **2004**, *13*, 296−298.
(42) Kaiser, A. B.; Duesberg, G.; Roth, S. *Phys. Rev. B* **1998**, *57*, 1418−1421.

Table 2. Mechanical Properties of HiPco SWNT Networks[a]

HiPco SWNTs	Young's modulus (MPa)	toughness (MJ/cm³)	tensile strength (MPa)	strain at break (%)
pristine	660	90	11	1.7
modified	950	830	37	4.3

[a] The modified networks were prepared from a suspension of nanotubes in $SOCl_2$.

on the relative significance of the barriers, with no temperature-induced phase transition or change in the nature of conduction. An analogous heterogeneous model seems particularly appropriate for entangled networks of ropes in $SOCl_2$-modified samples, where inter-rope contacts are likely to act as conduction barriers. $SOCl_2$ treatment appears to improve the conductivity by improving tube alignment and enhancing tube overlap, as seen in Figure 1.

Figure 2b represents the temperature dependence of the thermoelectric power measured for both pristine and chemically modified samples. These results provide experimental evidence for the shift of the Fermi level and the doping effect of $SOCl_2$ on the SWNTs. A positive sign of the thermopower indicates that holes are major charge carriers in both pristine and modified nanotube samples.

Mechanical Properties. One of the current applications of chemically modified bucky paper is in high-performance electromechanical actuators.[43] Consequently, mechanical properties of SWNT networks and their change upon $SOCl_2$ treatment are of high interest. Data presented in Table 2, which compare pristine and modified HiPco samples, demonstrate that chemical modification with $SOCl_2$ improves the measured mechanical properties of carbon nanotubes. Especially noteworthy is the increase in toughness by about 1 order of magnitude in the modified samples, prepared from a suspension of nanotubes in $SOCl_2$. The likely cause of the improved mechanical properties are $SOCl_2$-induced morphology changes in the SWNT networks, shown in Figure 1, which result in a denser nanotube packing due to an improved tube alignment and tube overlap.

Characterization of Chemically Modified Nanotubes. We showed in our previous work that exposure to $SOCl_2$ introduces considerable changes in the optical absorption spectra of both HiPco and laser ablation SWNTs. In particular, the absorption band at 0.75 eV, attributed to semiconducting tubes,[44] disappeared following chemical treatment. Raman spectroscopy results, presented in Figure 3, provide further evidence for chemical modification of the nanotubes. This observation goes along previous reports of Raman intensity changes of SWNTs in different chemical environments[10,45] or morphologies.[46] Spectra of the pristine samples exhibit asymmetry on the low-frequency side of the G band at ca. 1540 cm^{-1}. This asymmetry is related to the interaction of phonon excitations with the continuum electronic excitations and is called the Breit−Wigner−Fano (BWF) resonance. This effect is characteristic of metallic systems and therefore commonly attributed to metallic tubes.[47] Suppression of the BWF feature, observed in the modified samples, is assigned to the loss of continuum states due to chemical modification. Since chemical modification does not change the intensity of the D line at 1300 cm^{-1}, we expect the adsorbate−nanotube interaction to be noncovalent. This finding is in accord with the observed blue shift of the G line, which is indicative of an electron transfer from carbon to the adsorbate.

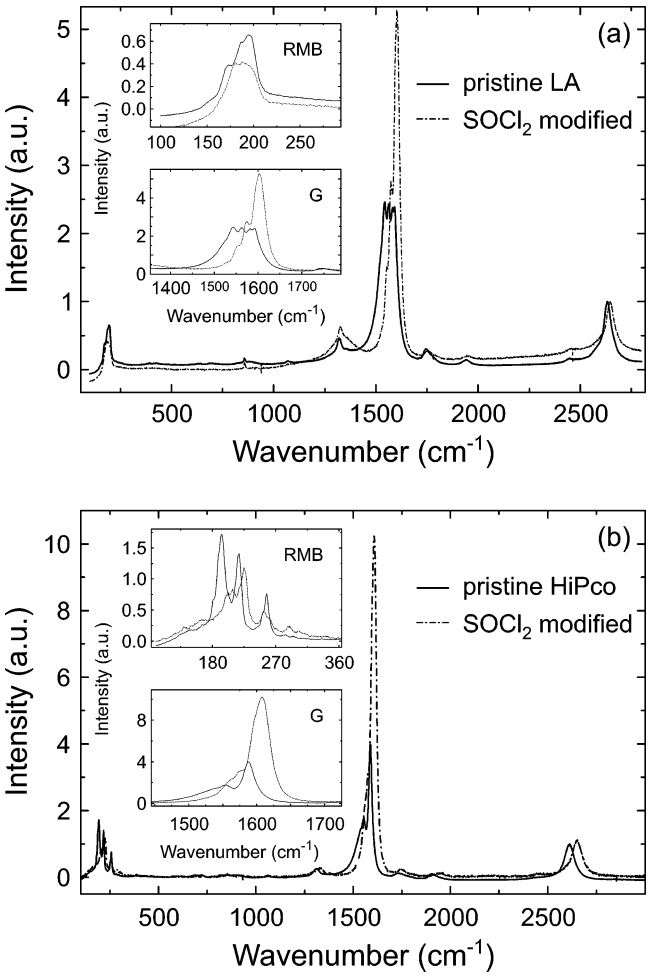

Figure 3. Changes in the Raman spectra of SWNTs produced by (a) laser ablation and (b) the HiPco process following exposure to $SOCl_2$.

Electronic and structural information about carbon atoms and local functionalities can be further deduced from the X-ray photoelectron spectra (XPS). Figure 4 shows changes in the core level spectra of SWNTs following chemical modification by $SOCl_2$. Using the tabulated cross sections for the photoemission process, we estimated the concentration of O, Cl, and S in the studied samples and present the corresponding results in Table 3.

These analysis results show that treatment with $SOCl_2$ induces significant changes in the sample composition. Approximately 4 at. % oxygen is detected in the pristine HiPco sample and 9 at. % in the pristine laser ablation (LA) sample. The oxygen concentration can be assigned to oxidized carbon sites, −COH, −C═O, and −COOH groups, or O_2 adsorbed on the surface. A higher amount of oxygen, up to 16 at. %, is noticed after reaction with $SOCl_2$. The oxygen concentration increase can be associated with the newly created species, e.g., SO_2 or SO_3, since the modified samples also show a relatively high concentration of sulfur of 3.3−3.9 at. %. Moreover, we detect

(43) Baughman, R. H.; Zakhidov, A. A.; De Heer, W. A. *Science* **2002**, *297*, 787−792.
(44) Dettlaff-Weglikowska, U.; Skakalova, V.; Graupner, R.; Ley, L.; Roth, S. *Mater. Res. Soc. Symp. Proc.* **2003**, *772*, *179*−*185.*
(45) Kavan, L.; Dunsch, L. *Nano Lett.* **2003**, *3*, 969−972.
(46) Heller, D. A.; Barone, P. W.; Swanson, J. P.; Mayrhofer, R. M.; Strano, M. S. *J. Phys. Chem. B* **2004**, *108*, 6905−6909.
(47) Brown, S. D. M.; Jorio, A.; Corio, P.; Dresselhaus, M. S.; Dresselhaus, G.; Saito, R.; Kneipp, K. *Phys. Rev. B* **2001**, *63*, 155414−1−155414−8.

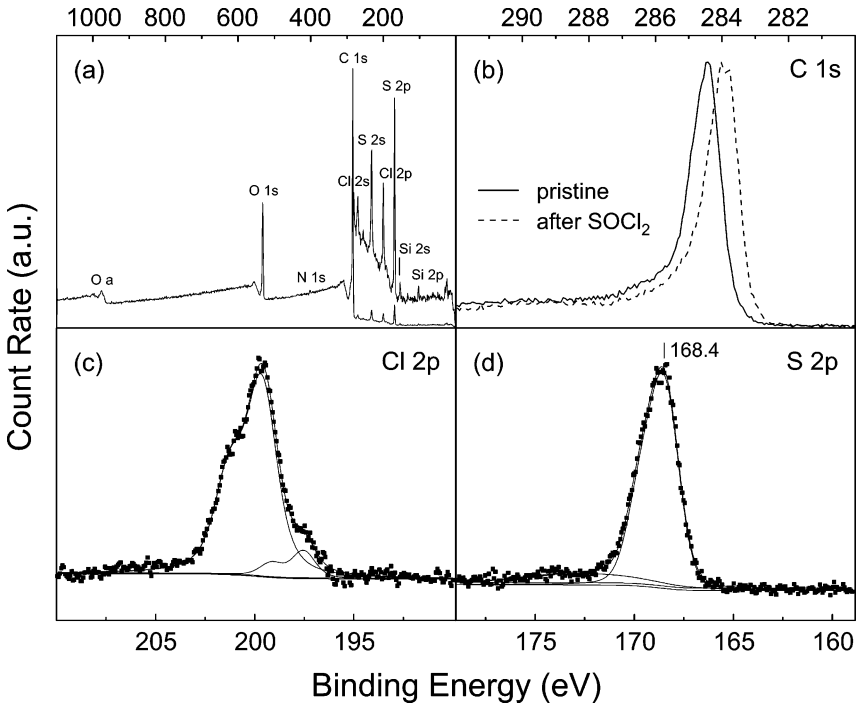

Figure 4. XPS core level spectra of SWNTs treated with $SOCl_2$: (a) full spectrum and spectra of (b) C 1s, (c) Cl 2p, and (d) S 2p core levels on an expanded energy scale.

Table 3. Concentration of O, Cl, and S in the Nanotube Samples, As Determined by XPS

SWNT sample	O (at. %)	Cl (at. %)	S (at. %)
HiPco pristine	4.2	0.45	
HiPco modified	15	0.8	3.3
LA pristine	9.1		
LA modified	16	1.9	3.9

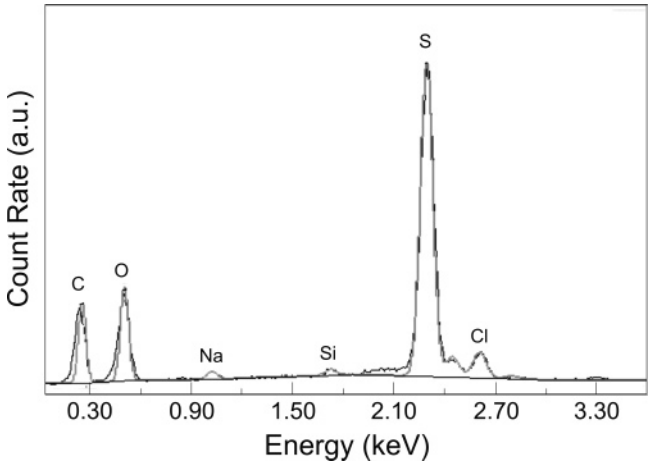

Figure 5. EDX spectrum of SWNTs produced by laser ablation after treatment with $SOCl_2$. Elemental composition of the sample (at. %): C, 65.25; O, 25.95; Na, 0.48; Si, 0.16; S, 7.17; Cl, 0.70; Co, 0.16; Ni, 0.14.

chlorine at 0.8 at. % in HiPco and 1.9 at. % in laser ablation samples following exposure to $SOCl_2$. These XPS elemental analysis results are confirmed by energy-dispersive X-ray analysis (EDX) results, presented in Figure 5, which also indicate increased amounts of oxygen, chlorine, and sulfur in the modified product.

Detailed analysis of the XPS spectra provides clear evidence that the SWNTs have been chemically modified. As seen in Figure 4b, the carbon C 1s peak, observed at 284.38 eV for sp^2 carbon in the pristine sample, is shifted by 0.4 eV to lower binding energy following chemical treatment. The chlorine Cl 2p core level spectrum, depicted in Figure 4c, reveals two inequivalent chlorine sites. The core level binding energies appear as doublets associated with 3/2 and 1/2 levels, which are separated by 1.6 eV due to spin−orbit coupling. The more intense Cl 2p component with a core level binding energy of 200.2 eV is typical of chlorine participating in organic C−Cl bonds. The less intense component with a lower binding energy of 198.8 eV can be assigned to chloride ions which are ionically bonded to the nanotube surface. The sulfur S 2p core level spectrum, shown in Figure 4d, also exhibits spin−orbit splitting but reveals only a single species with the S 2p 3/2 line situated at a binding energy of 168.4 eV. Unfortunately, assignment of this binding energy to a specific sulfur species is not straightforward. The S 2p binding energy in sodium dodecyl sulfate, used in the preparation of bucky paper, occurs at 168.8 eV, consistent with the literature data for S in the oxidation state +VI, as in SO_4^{-2}, which is usually observed at binding energies between 168.7 and 169.0 eV.[48] The binding energy of S 2p in the oxidation state +IV is reported to lie at 166.5 eV.[49] Therefore, the S 2p XPS signal observed in the modified samples can be assigned to intercalated $SOCl_2$ molecules, although we cannot exclude other S species, including SO_2, interacting with SWNTs. According to the base−acid theory of solution chemistry,[50] SO_2 could also provide SO^{2+} and SO_3^{2-} ions by self-ionization in aprotic solvents.

Complementary results to XPS are provided by near-edge X-ray absorption fine structure (NEXAFS) spectra. Figure 6 shows the C K-edge spectral region in the HiPco material. The

(48) Ruangchuay, L.; Schwank, J.; Sirivat, A. *Appl. Surf. Sci.* **2002**, *199*, 128−137.
(49) Beamson, G.; Briggs, D. *High-resolution XPS of Organic Polymers*; John Wiley & Sons: Chichester, 1992.
(50) *Gmelins Handbuch der Anorganischen Chemie;* Verlag Chemie GmbH: Weinheim 1963; Teil B, Nr. 9, p 315.

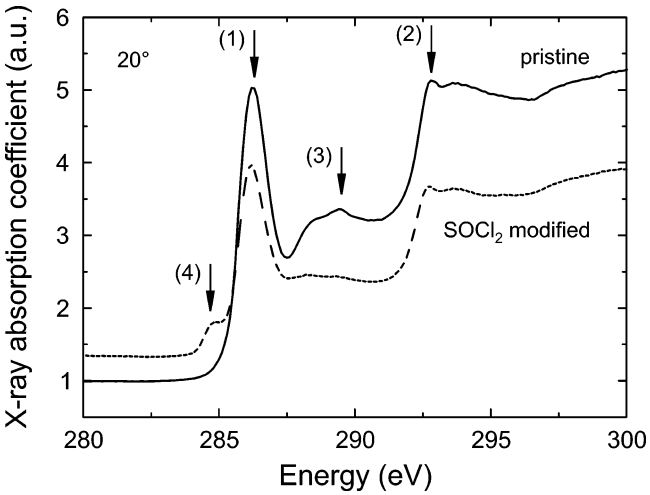

Figure 6. CKα-edge NEXAFS spectrum of the pristine and $SOCl_2$-modified HiPco sample.

spectrum is dominated by peak 1 at 286.2 eV, associated with π^* (ring) transitions, and peak 2 at 293.5 eV, associated with σ^* (ring) transitions. Two broad bands in region 3 are attributed to oxidized carbon functional groups. The band at 288.5 eV is identified with π^* states for C═O absorption of carbonyl groups, whereas the peak at 289.5 eV is attributed to σ^* states of C−O functionalities, similar to the assignment in oxidized HiPco samples and aromatic compounds with related substituents.[51] These two bands are strongly suppressed in the modified material. This fact suggests that $SOCl_2$ attacks oxidized groups and removes or replaces them with other groups. Following $SOCl_2$ treatment a new carbon species 4 appears at around 284.7 eV, on the left side of the carbon edge. We attribute this new peak to sp^2 carbons involved in the formation of charge-transfer complexes with sulfur-containing species. We propose the most likely reaction product to contain SO groups interacting with double bonds or structural defects in carbon nanotubes.

We also point out that $SOCl_2$ reacts with water at room temperature and decomposes to HCl and SO_2. Keeping the system free from water exposure would be a way of separating the direct effects of $SOCl_2$ from those of its hydrolysis products. Since our present experimental data do not distinguish effects that are to be attributed to $SOCl_2$ alone from those due to any of these species, we are planning a follow-up study under inert-gas atmosphere to shed more light on the direct role played by $SOCl_2$.

5. Theoretical Results

The optimized geometry of $SOCl_2$ interacting with a pyrene molecule, representing a nanotube fragment, is depicted in Figure 7a. $SOCl_2$ adsorbs preferentially with the SO axis parallel to a C−C bond. The distance of 2.7 Å between S and its closest C neighbor and the even shorter distance of 2.6 Å between O and its closest C neighbor are consistent with a relatively weak, partly ionic bond energy of 0.8 eV of $SOCl_2$ on pyrene, as shown in Table 4. The initial C−C distance of 1.42 Å in the center of pyrene, essentially identical to graphite and nanotubes, does not change upon chemisorption of $SOCl_2$. As seen in Table 4, the small distortion of the pyrene molecule following $SOCl_2$ chemisorption does not affect either the adsorption energy or the local adsorption geometry. Since a very similar adsorption geometry and chemisorption energy of $SOCl_2$ is found on the smaller naphthalene molecule also, we expect the adsorption geometry and energy on graphite fragments and carbon nanotubes to be essentially the same.

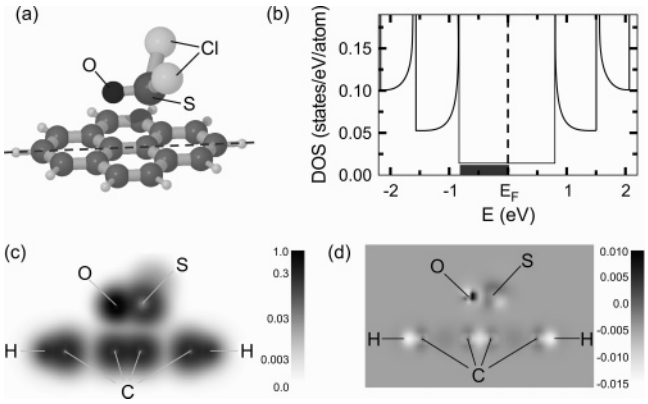

Figure 7. (a) Equilibrium structure of an $SOCl_2$ molecule adsorbed on a pyrene molecule representing a carbon nanotube segment. (b) Electronic density of states of a pristine (10,10) carbon nanotube with $E_F = 0$. (c) Total change density ρ_{tot} of the system in a plane which intersects the pyrene molecule at the dashed line and contains the S and O atoms. (d) Difference charge density $\Delta\rho = \rho_{tot} - \Sigma\rho_{at}$ in the same plane as defined in c, indicating regions of charge depletion and accumulation with respect to a superposition of neutral atoms. The scale bars in c and d are in e/au^3 units.

Table 4. Chemisorption Energy E_{ad} and Net Charge Transfer ΔQ from the Graphitic Substrate to the $SOCl_2$ and SO Adsorbates

system	E_{ad} (eV)	ΔQ (e)
SO/naphthalene	1.36	−0.11
$SOCl_2$/naphthalene	0.84	−0.16
SO/pyrene	1.34	−0.10
$SOCl_2$/pyrene	0.77	−0.06
$SOCl_2$/pyrene (rigid)	0.67	−0.06

Table 4 indicates that the binding energy between the SO radical and the graphitic fragment is about 0.5 eV stronger than for the related $SOCl_2$ molecule. The SO radical bonds preferentially with the sulfur atom bridging the C−C bond and with its axis perpendicular to the closest C−C bond. Still, SO lies nearly parallel to the graphitic surface. The oxygen atom in SO is farther away from the surface, close to the 6-fold hollow site of the carbon ring.

The charge distribution in $SOCl_2$ adsorbed on pyrene is shown in Figure 7c in a plane containing S, O, and the closest C−C bond. According to Table 4 there is a net charge transfer of about 0.1 electrons from naphthalene and pyrene to the $SOCl_2$ and SO adsorbates interacting with naphthalene and pyrene. Figure 7d, displaying the charge flow in the system, suggests that the largest charge accumulation occurs on oxygen and charge depletion is nearly uniform across the pyrene.

The effect of charge depletion on the electronic structure of the graphitic substrate is addressed in Figure 7b, which depicts the electronic density of states of a (10,10) carbon nanotube. Since adsorption of SO and $SOCl_2$ is primarily ionic in character, we will neglect adsorbate-induced changes in the electronic density of states of the nanotube in the following discussion. Even though the (10,10) nanotube is metallic, the electronic density of states $N(E_F)$ at the Fermi level is very low, close to 0.01 states/eV/atom. Assuming that the nanotube is not isolated

(51) Kuznetsova, A.; Popova, I.; Yates, J. T., Jr.; Bronikowski, M. J.; Huffman, C. B.; Liu, J.; Smalley, R. E.; Hwu, H. H.; Chen, J. G. *J. Am. Chem. Soc.* **2001**, *123*, 10699−10704.

and interacts with other nanotubes as well as SO or $SOCl_2$, we may safely consider the electronic transport to be diffusive with conductance proportional to $N(E_F)$. Obviously, shifting the Fermi level into the region of the first van Hove singularity at −0.8 eV should enhance $N(E_F)$ and the conductivity significantly. In semiconducting nanotubes this is achieved even with a negligible charge transfer. Even in pristine metallic nanotubes, in view of the low value of $N(E_F)$, the necessary charge transfer amounts to a charge depletion of only 0.008 electrons per carbon atom. In view of the charge transfer of 0.1 electrons per adsorbate, only one SO or $SOCl_2$ per 10 carbon atoms should be sufficient to achieve such a change. Since only one-third of the nanotubes are expected to be metallic on average, the expected loading level, which should shift the Fermi level into the van Hove singularity region in all nanotubes, should amount to about 1 SO or $SOCl_2$ per 30 carbon atoms. This estimate is in very good agreement with the observed conductivity increase following a loading level, which translates into one $SOCl_2$ molecule per 10−20 carbon atoms, in rough agreement with the elemental analysis presented in Table 3.

6. Conclusions

We studied a new method to chemically modify entangled single-wall carbon nanotube networks, called bucky paper. We found that treatment by thionyl chloride, $SOCl_2$, provides a simple way to significantly improve the electrical conductivity and mechanical properties of bucky paper. We characterized the chemical modification using SEM, XPS, NEXAFS, EDX, and Raman spectroscopy measurements and ab initio calculations. We found that formation of charge-transfer complexes within the nanotube bundles leads to a charge redistribution in the system, resulting in electron depletion of the sp^2-bonded carbon nanotubes. This *p*-type doping effect is consistent with electronic structure calculations, which indicate a Fermi level shift into the valence band, and is confirmed by the temperature dependence of the thermopower. We observe an increase by up to factor of five in the electrical conductivity of the chemically modified sample at room temperature and an even more pronounced increase at lower temperatures. This transition from semiconducting to metallic behavior is accompanied by a similar improvement in the mechanical properties of nanotube networks, which is attributed to improved alignment and enhanced overlap of nanotubes in the chemically treated bucky paper.

Acknowledgment. This work was jointly supported by the European Commission's Fifth Framework Program (CARDECOM Project Contract No. G5 RD-CT-2002-00585) and by the Sixth Framework Program (SPANG Project Contract No. NMP4-CT-2003-505483), by KISTEP (Contract No. M6-0301-00-0005, Korea), by the NSF-NIRT (grant no. DMR-0103587), and the NSF NSEC (grant no. 425826). We gratefully acknowledge the assistance of Monika Riedl and Uve Vorher of the Fraunhofer Institut für Grenzflächen und Bioverfahrenstechnik in Stuttgart, Germany, with the SEM images.

JA046685A